A fluorescent microporous crystalline dendrimer discriminates vapour molecules

doi: 10.1039/C7CC09342J

Journal Name

COMMUNICATION

A fluorescent microporous crystalline dendrimer discriminates vapour molecules

Received 00th January 20xx,
Accepted 00th January 20xx

DOI: 10.1039/x0xx00000x

www.rsc.org/

Sae Nakajima,[a†] Ken Albrecht,[bc†] Soh Kushida,[ad†] Eiji Nishibori,[ef] Takashi Kitao,[gh] Takashi Uemura,[gh] Kimihisa Yamamoto,[gh] Uwe H. F. Bunz,*[d] Yohei Yamamoto*[af]

A self-assembled crystalline microporous dendrimer framework (MDF) exhibits novel turn-on and ratiometric fluorescence upon exposure to solvent vapours. The donor-acceptor character, combined with the large surface area (> 650 m^2 g^{-1}), allows the MDF to discriminate vapours of volatile solvents with turn-on and colour change of photoluminescence.

Fluorescent probes detect vastly different analytes, including nerve gases, heavy metal ions, proteins, and can even monitor gene expression – to name a few examples.[1] There are several types of fluorescent sensing; quenching, fluorescence turn on and ratiometric, in addition to specialized FRET-schemes etc.[2] In quenching and turn on, sensing is evaluated by the intensity change of the fluorescence at a specific fluorescence wavelength; detection of several analytes is difficult if one uses only a single probe. Therefore, for practical applications, solid-state fluorescent sensors with fluorescence colour change are attractive, as they add a dimension to the discriminative power and allow inspection by eye. A highly porous medium with large surface area and nanometre size channels is favoured for gas and vapour sensing as the analytes can access pores and the interior of the medium.[3]

Here, we report a crystalline framework from a π-conjugated dendrimer **1** with a molecular weight of 3,778 Da composed of an electron-accepting triazine (TAZ) core and electron-donating carbazole (Cz) dendrons (Figs. 1a and S1).[4] This electronic structure results in a small energy difference between the S_1 and T_1 levels (ΔE_{S-T}) in the charge-transfer (CT) excited state (< 0.1 eV). Most dendrimers are amorphous in the solid state – particularly those of higher generation.[5] Our π-conjugated dendrimer forms crystalline fibres with quasi-one-dimensional (1D) nanopores along its long axis. Because of the highly porous structure, combined with the donor-acceptor character, the dendrimer exhibits enhanced photoluminescence (PL) accompanied by colour change upon exposure to solvent vapours, allowing to sense and discriminate them.

The self-assembly behaviour of **1** was investigated by slow diffusion of poor solvents such as acetonitrile (MeCN), acetone, and methanol (MeOH) into a chloroform ($CHCl_3$) solution of **1** with a systematic change of the initial concentration.[6] Upon diffusion of acetonitrile vapour into the dilute solution of **1** in $CHCl_3$ ([**1**] = 0.1 mg mL^{-1}), a pale-yellow precipitate was obtained, composed of well-defined microspheres with a diameter range from 2 to 8 μm (Fig. 1b, SEM). By contrast, when the initial concentration of **1** was increased to 1.0 mg mL^{-1}, diffusion of acetonitrile vapour resulted in the precipitation of thin fibres with widths of several micrometres and lengths > 100 μm (Fig. 1c). The limit of the initial concentration for the different morphologies is between 0.1 and 0.5 mg mL^{-1} (Fig. S2a). MeOH as a polar nonsolvent exclusively produced microspheres at concentrations up to 10 mg mL^{-1} (Fig. S2c).

As revealed by detailed self-assembly studies, microfibres of **1** in the $CHCl_3$/MeCN mixed solvent is thermodynamically more stable than microspheres (Figs. S3 and S4). In high concentration condition ([**1**] = 1.0 mg mL^{-1}), microfibres start to form at the vapour diffusion period (t_{VD}) of ~33 h (Fig. S3b–i). On the other hand, in the dilute condition ([**1**] = 0.1 mg mL^{-1}), microspheres start to form at t_{VD} ~39 h, which is much later than the precipitation in the high concentration condition (Fig. S3j–q). Interestingly, when the vapour diffusion is stopped at t_{VD} = 39–42 h and the resultant microsphere suspension is

[a] Division of Materials Science, Faculty of Pure and Applied Sciences, University of Tsukuba, 1-1-1 Tennodai, Tsukuba, Ibaraki 305-8573, Japan.
[b] Laboratory for Chemistry and Life Science, Tokyo Institute of Technology, 4259 Nagatsuta Midori-ku, Yokohama 226-8503 Japan.
[c] ERATO Yamamoto Atom Hybrid Project, Japan Science and Technology Agency (JST), 4259 Nagatsuta Midori-ku, Yokohama 226-8503 Japan.
[d] Organisch-Chemisches Institut, Ruprecht-Karls-Universität Heidelberg, Im Neuenheimer Feld 270, 69120 Heidelberg, Germany.
[e] Division of Physics, Faculty of Pure and Applied sciences, University of Tsukuba, 1-1-1 Tennodai, Tsukuba, Ibaraki 305-8573, Japan.
[f] Tsukuba Research Centre for Energy Materials Science (TREMS), University of Tsukuba, 1-1-1 Tennodai, Tsukuba, Ibaraki 305-8573, Japan.
[g] Department of Synthetic Chemistry and Biological Chemistry, Graduate School of Engineering,, Kyoto University, Katsura, Nishikyo-ku, Kyoto 615-8510, Japan.
[h] CREST, JST, 4-1-8 Honcho, Kawaguchi, Saitama 332-0012, Japan.
† These authors equally contribute to this work.
Electronic Supplementary Information (ESI) available: [details of any supplementary information available should be included here]. See DOI: 10.1039/x0xx00000x

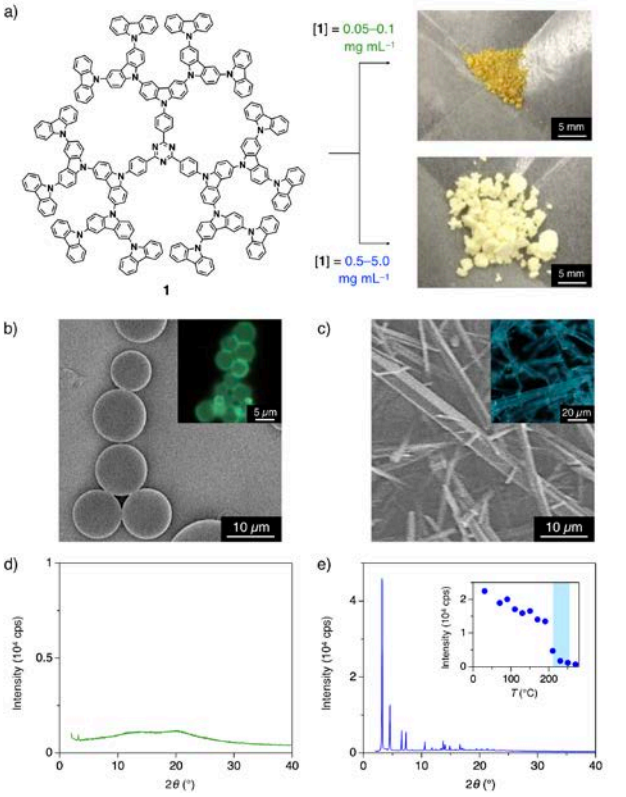

Fig. 1. (*a*) Molecular structure of **1** and photographs of powder samples of self-assembled precipitates prepared by a vapour diffusion of acetonitrile into $CHCl_3$ solutions of **1** with initial concentrations of 0.1 (right-top) and 1.0 mg mL^{-1} (right-bottom). The weights of the powder samples in the photographs are 20.046 mg (right-top) and 20.014 mg (right-bottom). (*b*, *c*) SEM micrographs of self-assembled spheres (b) and fibres (c) of **1**, prepared by vapour diffusion of acetonitrile into $CHCl_3$ solutions with initial concentrations of 0.1 and 1.0 mg mL^{-1}, respectively. Insets show fluorescence micrographs of the self-assembled spheres (b) and fibres (c) of **1**. λ_{ex} = 340–390 nm. (*d*, *e*) XRD patterns of the self-assembled spheres (d) and fibres (e) of **1**. X-ray source: Cu$K\alpha$. The inset in (e) shows a plot of the peak intensity at 2θ = 3.19° upon heating from 30 to 270 °C.

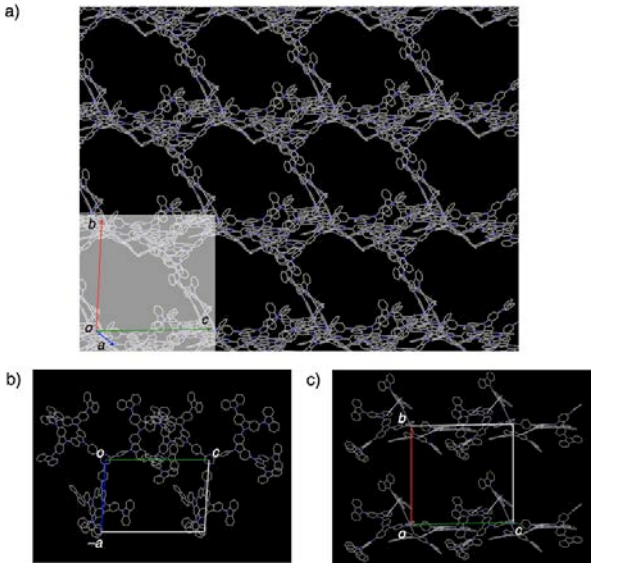

Fig. 2. (*a*) Proposed packing structure of 1 in the self-assembled fibres. The quasi-1D micropores penetrate through the long axis of the fibres (*a*-axis direction). (*b*, *c*) Lattice structures viewed from ***b*** (b) and ***a*** (c) axis directions.

allowed to incubate for one week, microspheres transform into microfibres (Fig. S3n' and o'). On the other hand, in case that t_{VD} is longer than 50 h, microsphere-to-microfibre transformation hardly occurs (Fig. S3p' and q'). From the overall analysis on dissolution (Fig. S4a and b) and reprecipitation studies (Fig. S4c–g), microfibres are more stable than microspheres in the $CHCl_3$/MeCN mixed solvent. However, microspheres form very quickly, whereas the microfibres grow sluggish. Therefore, once microspheres form in a dilute condition and the fraction of the nonsolvent increases in the vapour diffusion process, the kinetically trapped microsphere morphology preserves without transforming to microfibres.

1 is amorphous in its microsphere form, according to powder X-ray diffraction (XRD, Fig. 1d). By contrast, the fibres are crystalline with sharp diffraction peaks in the XRD pattern (Fig. 1e). Synchrotron radiation (SR) X-ray diffraction (SR-XRD) of a single piece of the fibre (dimensions: 300 × 30 × 15 μm^3) reveals clear diffraction spots (Fig. S5), and the crystal is assigned to a triclinic (*P*1) system (Tables S2 and S3). However, the crystal is twinned with several directions on the *b*-*c* plane. The diffraction spots indicate a plate-like two-dimensional (2D) crystal with a very short correlation length, therefore the packing structure of **1** is difficult to solve from the single-crystal XRD data.

Alternatively, the packing of **1** in the fibre is investigated by SR powder XRD using the direct-space strategy.[7a] A genetic algorithm (GA) solves the structure.[7b] Based on the reliability factors of the powder profiles, the most plausible packing is determined (Figs. 2a–c and S6). Molecules of **1** assemble into 2D layers with quasi-1D, nanometre-sized pores along the direction of the *a*-axis, forming a microporous structure. The potential pore volume percentage is as large as 71.3% (pore volume 8,790 Å per cell volume 12,327 Å). The intermolecular interaction between the Cz moieties is small, and each molecule of **1** is almost isolated. In a macroscopic view of the powder samples, the fibres of **1** appear like a fabric-type powder due to their high porosity, a contrast to the dense sandy powder of the amorphous spheres of **1** (photograph in Fig. 1a).

In the differential scanning calorimetry (DSC) traces, the amorphous spheres of **1** show no characteristic endothermic/exothermic behaviour (Fig. S7a). By comparison, the fibres exhibit an exothermic peak at 230 °C in the first heating process, whereas no peak appears in the second cycle (Fig. S7b). An abrupt decrease in the intensity of the diffraction peaks of the microfibres of **1** is observed above 200 °C (Figs. 1e inset and S8), indicating the transition of **1** from crystalline to the amorphous state. As mentioned, crystalline microfibres are energetically preferred to amorphous microspheres in

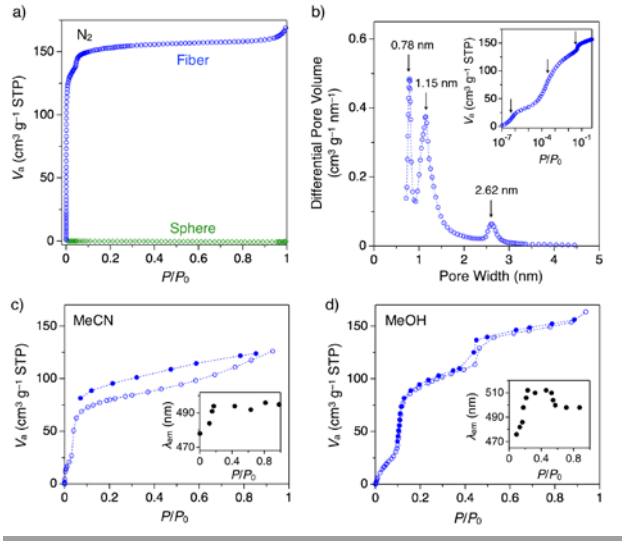

Fig. 3. (*a*) N_2 sorption isotherms at 77.3 K for self-assembled fibres (blue) and spheres (green) of **1**. (*b*) Plot of differential pore volume versus pore width for self-assembled fibres of **1**. The inset shows the N_2 sorption isotherm at the low-pressure region. The saturated vapour pressures (P_0) of N_2 at 77.3 K is 101.3 kPa. (*c*, *d*) Gas and vapour sorption isotherms of self-assembled fibres of **1** at 298 K for acetonitrile (c) and MeOH (d). Open and closed circles indicate sorption and desorption processes, respectively. Saturated vapour pressures (P_0) of MeCN and MeOH at 298 K are 11.8 and 17.05 kPa, respectively. Insets show plots of λ_{em} versus P/P_0 of acetonitrile (c) and MeOH (d).

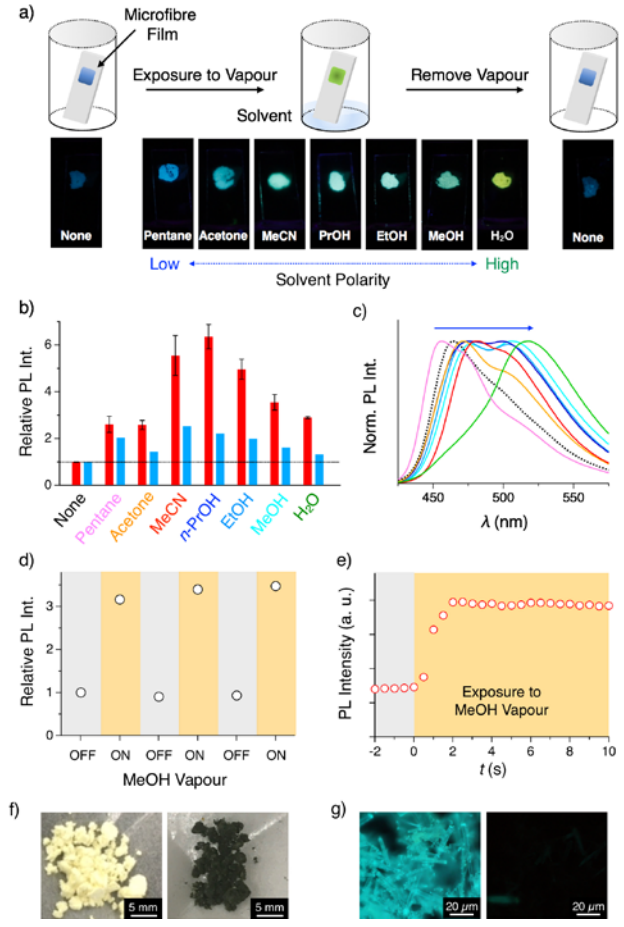

Fig. 4. (*a*) Schematic representation of the introduction/removal of solvent vapours and the corresponding fluorescent microscope images of cast films of the porous microfibres of **1**. (*b*) Bar graphs of the PL area intensity of cast films of the porous microfibres of **1** in solvent vapour relative to that without solvent vapour. Red, in air; blue, in argon. (*c*) Normalized PL spectra of cast films of the porous microfibres of **1** in air (dotted curve) and in the solvent vapours (solid curves). The colour of the spectra corresponds with the colour of the description of the solvents in b). (*d*) Plot of the relative area intensity of the PL spectra of a cast film of microfibres of **1** with (on) and without (off) MeOH vapour repeatedly. (*e*) Time dependence of the PL intensity of the microfibres of **1** upon exposure to MeOH vapour. (*f*, *g*) Photographs (f) and fluorescent micrographs (g) of microfibres of **1** before (left) and after (right) penetrating TCNQ.

$CHCl_3$/MeCN cosolvent. However, the DSC results indicate that, once the solvent is removed from the pores, the crystalline state becomes thermodynamically less stable than the dense amorphous state.

Fibres and spheres of **1** display contrasting PL characteristics. Fibres show blue PL with a maximum wavelength (λ_{em}) of 482 nm and a shoulder at 461 nm (Figs. 1c inset and S9a), matching with that of a toluene solution of **1** (λ_{em} = 473 nm).[4] The spheres display greenish PL (λ_{em} = 492 nm, Figs. 1b inset and S9a). These spectroscopic results indicate that **1** experiences intermolecular π-electronic interactions in the spheres compared to that in the crystalline fibres. PL spectra are also affected by the polarity of solvent, due to the CT character of **1** (Fig. S9b).[4,8]

The nitrogen (N_2) isotherm of the porous fibres displays a three-step uptake behaviour with the highest reported porosity of assembled dendrimers (Fig. 3a blue, S_{BET} = 664.5 m^2 g^{-1}). From the *T*-plot analysis, 99% of the adsorbed surface (657.8 m^2 g^{-1}) originates from the pores inside the fibres. From the analysis in the low-pressure region, the pore widths are determined as 0.78, 1.15, and 2.62 nm (Fig. 3b), matching with the pore size determined by XRD (Fig. 2c). The amorphous spheres, in contrast, display negligible gas sorption behaviour (Fig. 3a, green).

Similar to the N_2 sorption profile, vapours of acetonitrile and MeOH display multistep sorption profiles for the fibres, with total uptake amounts comparable to that of N_2 (Fig. 3c and d). Increasing sorption of acetonitrile and MeOH increases the red shift of λ_{em} (Figs. 3c,d inset and S10a,b), which also accompanies changes of the XRD patterns (Fig. S10c and d).

We exposed films of the porous fibres to different solvent vapours (Fig. 4a). Their fluorescence intensity is greatly enhanced (Fig. 4b, red), and the fluorescent colours change (Fig. 4a and c). The PL colour shift follows the strength of the solvent polarity; the CT excited state is stabilized by the adsorption of polar solvents. The turn-on may be caused by the suppression of energy transfer from the triplet excited state of **1** to the triplet oxygen in the dry pores. Purging the fibres with argon suppresses the enhancement of the fluorescence intensity, supporting this hypothesis (Fig. 4b, blue). The PL change is reversible for the fibre (Figs. 4d and

S11), but non-porous films and microspheres do not show this effect at all (Fig. S12). Upon exposure to vapour, the change of the PL intensity is complete within 2 s (Fig. 4e). In case where the porous fibres are exposed to the vapours of MeOH/H_2O mixture, the PL intensity enhancement is much greater than in the case of the exposure to each solvent (Fig. S13). The PL colour shifts depending on the mixing fraction of MeOH and H_2O.

Vapour of the electron-accepting 7,7,8,8-tetracyanoquinodimethane (TCNQ) penetrates the porous fibres (fibres and TCNQ are combined in a glass tube, weight ratio, 1 : 5, sealed and heated at 150 °C for 3 h, Fig. S14a and b). The colour of the fibres changes from pale yellow to dark green, and new CT absorption bands appear in the visible range (Fig. S14c). The fluorescence is completely quenched caused by the electron transfer from carbazole to TCNQ (Fig. 4f,g). However, their XRD pattern remains almost unchanged, indicating that the fibres retain their order upon filling (Fig. S15). According to the ^{1}H-NMR of dissolved fibres, the ratio of the penetrated TCNQ to **1** increases as the amount of the sealed TCNQ in the glass tube increases and saturates to a ration of ~4/1 (Fig. S16). Heating in the open, TCNQ is removed from the pores, restoring the PL to the original state (Fig. S17). We also confirm that other molecules such as 2,3,5,6-tetrafluoro-7,7,8,8-tetracyanoquinodimethane (F4-TCNQ) and pyrene can be introduced into the nanochannels of the microfibres of **1** by the similar sublimation treatment (Figs. S18 and S19).

In summary, we prepare fibres of **1** with quasi-1D nanopores with surface area as large as 650 m^2 g^{-1} by non-solvent precipitation; this is in distinct contrast to the amorphous microspheres where **1** is densely packed. Due to the highly porous structure in the donor-acceptor dendrimer crystal, vapours of non-solvents efficiently penetrate the nanochannels and turn on the fluorescence with colour change, depending on the polarity of the incorporated solvent molecules. Electron-accepting TCNQ and F4-TCNQ also penetrate the nanochannels, leading to dramatic colour change and PL quenching. This work paves the way to discriminate volatile gases and organic molecules, utilizing attractive donor-acceptor π-conjugated dendrimers. Discrimination and detection of nitroarenes, amines, solvents etc. are future directions to pursue.[9]

Acknowledgements

This work was supported by a Grant-in-Aid for Scientific Research on Innovative Areas "π-System Figuration" (JP17H05142, JP17H05146), “Coordination Asymmetry” (JP16H06517), Scientific Research (A) (JP16H02081), and Scientific Research (S) (JP15H05757) from Japan Society for the Promotion of Science (JSPS), University of Tsukuba Pre-strategic initiative “Ensemble of light with matters and life”, Asahi Glass Foundation, JST CREST program (JPMJCR1321), and DAAD (Doctoral Programmes, No. 91612715). The synchrotron radiation experiments were performed at SPring-8 with the approval of the Japan Synchrotron Radiation Research Institute (JASRI) as a Partner User (Proposal No: 2015A0074 and 2014A0078).

Conflicts of interest

There are no conflicts to declare.

Notes and references

1 (*a*) O. R. Miranda, C.-C. You, R. Phillips, I.-B.; Kim, P. S. Ghosh, U. H. F. Bunz, V. M. Rotello, *J. Am. Chem. Soc.* 2007, **129**, 9856; (*b*) C. Ornelas, R. Pennell, L. F. Liebes, M. Weck, *Org. Lett*. 2011, **13**, 976; (*c*) X. Li, X. Gao, W. Shi, H. Ma, *Chem. Rev.* 2014, **114**, 590; (*d*) U. H. F. Bunz, J. Kumpf, J. Freudenberg, *Analyst* 2015, **140**, 3136.

2 (*a*) J. R. Askim, M. Mahmoudi, K. S. Suslick, *Chem. Soc. Rev.* 2013, **42**, 8469; (*b*) M. A. Saeed, H. T. M. Le, O. S. Miljanic, *Acc. Chem. Res*. 2014, **47**, 2074; (*c*) J. Wu, B. Kwon, W. Liu, E. V. Anslyn, P. Wang, J. S. Kim, *Chem. Rev*. 2015, **115**, 7893.

3 (*a*) S. Hecht, J. M. J. Fréchet, *Angew. Chem. Int. Ed*. 2001, **40**, 74; (*b*) L. E. Kreno, K. Leong, O. K. Farha, M. Allendorf, R. P. Van Duyne, J. T. Hupp, *Chem. Rev.* 2012, **112**, 1105; (*c*) Z. Hu, B. J. Deibert, J. Li, *Chem. Soc. Rev*. 2014, **43**, 5815; (*d*) C. Gu, N. Huang, J. Gao, F. Xu, Y. Xu, D. Jiang, *Angew. Chem. Int. Ed*. 2014, **53**, 4850; (*e*) X. Zhang, J. Lu, J. Zhang, *Chem. Mater*. 2014, **26**, 4023; (*f*) N. Huang, P. Wang, D. Jiang, *Nat. Rev. Mater.* 2016, **1**, 16068; (*g*) W. P. Lustig, S. Mukherjee, N. D. Rudd, A. V. Desai, J. Li, S. K. Ghosh, *Chem. Soc. Rev.* 2017, **46**, 3242; (*h*) A. Pulido, L. Chen, T. Kaczorowski, D. Holden, M. A. Little, S. Y. Chong, B. J. Slater, D. P. McMahon, B. Bonillo, C. J. Stackhouse, A. Stephenson, C. M. Kane, R. Clowes, T. Hasell, A. I. Cooper, G. M. Day, *Nature* 2017, **543**, 657.

4 K. Albrecht, K. Matsuoka, K. Fujita, K. Yamamoto, *Angew. Chem. Int. Ed*. 2015, **54**, 5677-5682.

5 (*a*) R. E. Bauer, V. Enkelmann, U. M. Wiesler, A. J. Berresheim, K. Müllen, *Chem. Euro. J.* 2002, **8**, 3858; (*b*) D. Wassenfallen, G. Mattersteig, V. Enkelmann, K. Müllen, *Tetrahedron* 2006, **62**, 5417-5420. (*c*) Z. Pan, M. Xu, E. Y. Cheung, K. D. M. Harris, E. C. Constable, C. E. Housecroft, *J. Phys. Chem. B* 2006, **110**, 11620.

6 (*a*) S. Kushida, D. Braam, T. D. Dao, H. Saito, K. Shibasaki, S. Ishii, T. Nagao, A. Saeki, J. Kuwabara, T. Kanbara, M. Kijima, A. Lorke, Y. Yamamoto, *ACS Nano* 2016, **10**, 5543; (*b*) S. Kushida, O. Oki, H. Saito, J. Kuwabara, T. Kanbara, M. Tashiro, M. Katouda, Y. Imamura, Y. Yamamoto, *J. Phys. Chem. Lett.* 2017, **8**, 4580.

7 (*a*) K. D. M. Harris, M. Tremayne, P. Lightfoot, P. G. Bruce, *J. Am. Chem. Soc.* 1994, **116**, 3543; (*b*) E. Nishibori, T. Ogura, S. Aoyagi, M. Sakata, *J. Appl. Cryst.* 2008, **41**, 292.

8 C. Reichardt, *Chem. Rev*. 1994, **94**, 2319-2358.

9 (*a*) G. Tang, S. S. Y. Chen, P. E. Shaw, K. Hegedus, X. Wang, P. L. Burn, P. Meredith, *Polym. Chem*. 2011, **2**, 2360; (*b*) Y. Geng, M. A. Ali, A. J. Clulow, S. Fan, P. L. Burn, I. R. Gentle, P. Meredith, P. E. Shaw, *Nat. Commun*. 2015, **6**, 8240.

